Modelling optical coherence tomography for biophotonics and photobiology using an electronically tunable mode-locked laser diode

I. Ejidike[c], S. Shutts[d], D. Bajek*[a,b]

[a] Photobiology Unit, NHS Tayside, Ninewells Hospital, Dundee, U.K.; [b] School of Medicine, University of Dundee, Dundee, U.K.; [c] Institute of Photonics and Quantum Sciences, Heriot-Watt University, Edinburgh, UK, EH14 4AS; [d] School of Physics and Astronomy, Cardiff University, Cardiff, U.K

*Email: dbajek001@dundee.ac.uk

ABSTRACT

We propose mode-locked laser diodes (MLLDs) for their deployment in a low-cost and portable optical coherence tomography (OCT) system. OCT is an essential imaging technique used for medical diagnoses in dermatology, ophthalmology, and cardiology. Based on low-coherence interferometry, OCT directs infrared light through various layers of tissue, which is reflected onto a detector and resolved as an image. Generally, swept-source OCT (SS-OCT) systems perform better than grating based systems and time domain OCT but require expensive laser sources which are optically pumped, meaning they require an additional pump laser, limiting their deployment in clinics. To that end we propose MLLDs as an excellent candidate to realize, low-cost, compact, and portable SS-OCT enabled by their fast electronic tuning and electrically pumped, monolithic construction. We present simulated SS-OCT images using experimentally measured spectra from our InAs Quantum-Dot MLLDs and compare this to simulated data using a Thorlabs research-grade micromechanically tuned VCSEL (vertical cavity surface emitting lasers). Our first results to date suggest MLLDs could resolve features of 62.5 μm, which, compared with the off-the-shelf system, is approximately half the resolution. Further studies suggest that by examining electronic fine-tuning of the spectral linewidths and central wavelength, MLLDs may be highlighted as a key tool in realizing low-cost portable OCT at comparable quality to existing research-grade systems. Couple this with the current shift in practices to complex image analysis using machine learning methods, a handheld SS-OCT system could be realized as a low-cost, compact and versatile tool for clinicians.

Keywords: MLLD, OCT, SLASOPS, OSBERT, Biophotonics, Photobiology

1. INTRODUCTION

1.1 Motivation

Optical coherence tomography (OCT) offers itself as a convenient solution to high-resolution close-range depth sensing and 3D imaging in biophotonics[1-4]. Time-domain OCT (TD-OCT) systems rely on an interferometric setup with large device footprints, where the resolution is limited by the optical pulse width and detector speeds. It has been shown that Fourier domain OCT (FD-OCT) measurements typically have a higher SNR (Signal-to-Noise Ratio)[5], and as such the state-of-the-art in both research and clinics has tended towards this modality of OCT.

Commercially, OCT systems are dominated by spectral domain (SD-OCT) setups[6] that use a grating to interrogate the spectral information of the signal which is then Fourier-Transformed to resolve timing and depth information. Swept source methods (SS-OCT) resolve spectral information by instead tuning the frequency of the source which allows the use of compact, lower cost one-dimensional detectors, and generally the performance of SS-OCT systems outperforms SD-OCT[7]. As such we seek to investigate the implementation of a mode-locked laser diode (MLLD) as a tunable semiconductor source in swept source systems. We have previously demonstrated that the purely electronic tuning of these devices unlocks megahertz scan rates for time-resolved interferometric measurements[8, 9] and a similar "akinetic" semiconductor source has demonstrated competitive scan rates compared to the state of the art[10].

Compared to the vertical cavity surface emitting lasers (VCSELs) used in some SS-OCT systems, MLLDs offer a similar cost reduction (compared to solid-state alternatives), using a laser diode on the scale of millimeters. The benefits of MLLDs lie in their monolithic and versatile design. Due to the nature of the tuning they would not need an external k-clock to correctly sample scan points and are electronically pumped as opposed to being optically pumped, which could allow for extremely compact SS-OCT configurations at half the cost (i.e. no requirement for a secondary pump-laser). Simply biasing multiple sections of a MLLD and varying the voltage leads to spectral tuning, and the customizability of this range can be greatly enhanced by choosing which sections are biased (and across which positive or negative ranges). It has been demonstrated that MLLDs can achieve sub-nm linewidths[11] and to that end we believe that they could serve as a cost-effective source that could bring SS-OCT to clinic in a portable and durable format.

We therefore present our hybrid experimental and modelling work to showcase the potential of MLLDs and their deployment in biophotonics applications such as OCT. Previously we have experimentally demonstrated that changing bias voltage in difference sections of MLLDs can tune not only pulse repetition rate but also the frequency of the output[12], to that end we want to ascertain the viability of MLLDs for SS-OCT. Using the spectra from an MLLD fabricated in-house we use our simulation as a preliminary investigation into the efficacy of MLLDs as an SS-OCT source and to motivate more investigation into the development of the platform for SS-OCT.

1.2 Optical coherence tomography (OCT) theory

In FD-OCT systems in a standard 50:50 Michelson interferometer setup the depth resolution δz is related to the central wavelength λ_0 and the tuning range $\Delta\lambda$ of the source by

$$\delta z = \frac{\lambda_0^2}{2n_{avg}\Delta\lambda} \tag{1}$$

where n_{avg} is the average refractive index of the sample[13]. The range is limited two-fold by the sampling interval of the wavelengths $\delta_s\lambda$ and the linewidth of the source (or spectral resolution) $\delta\lambda$. The Fourier transform of the spectral data results in a maximum depth defined as[13]

$$z_{max} = \frac{\lambda_0^2}{4n_{avg}\delta_s\lambda} \tag{2}$$

But we also find that the signal sensitivity falls off at longer ranges due to the convolution of the source linewidth with the "true" signal spectrum, the 6 dB point (or coherence length) is then defined as[13]

$$z_{6dB} = \frac{\ln(2)}{\pi}\frac{\lambda_0^2}{\delta\lambda} \tag{3}$$

1.3 Mode-locked laser diode (MLLD)

Edge-emitting lasers with segmented contacts, illustrated schematically in figure 1, were fabricated from InAs quantum dot (QD) material emitting in the region of 1.2 – 1.3 μm. The epitaxial structure was grown by solid-source molecular beam epitaxy on an n-type GaAs substrate with an active region comprising five InAs/InGaAs dot-in-well (DWELL) layers each separated by 50 nm of GaAs, with the rest of the waveguide formed from 1200 nm cladding layers $Al_{0.40}Ga_{0.60}As$ on either side. Dry-etching was used to create broad area 100 μm wide mesas and Ti-Au p-type segmented contacts (50μm wide by 300 μm long) were formed using standard optical lithography, thermal evaporation and a lift-off process. A wet-etch procedure was used to remove the highly doped GaAs cap layer between the p-contacts to increase the electrical

resistance, allowing sections to be biased individually. The sample was thinned to 100 µm and a AuGe-Ni-Au contact was formed on the substate side, before cleaving to 3000 µm long cavities.

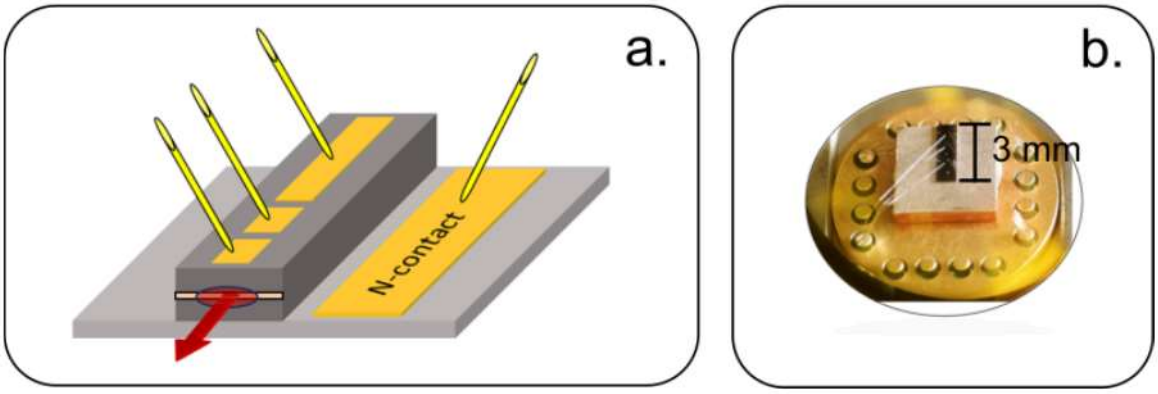

Figure 1. (a) Schematic of our edge emitting laser, showing the different biased sections (b) Color image of our source, showcasing monolithic construction and small form factor.

Measurements were carried out pulsed, with a 1kHz repetition frequency and 1µs pulse width, to mitigate the effects of self-heating and prevent any thermal tuning with applied bias. The front two sections of the device were connected together and driven by a single current source with the remaining rear sections being driven by a second source. To set the initial conditions for tuning the emission spectra, the current supplied to the rear sections (I_2) was increased until the onset of lasing was achieved, with the front two sections floating (unbiased). The current in the front two sections was then increased, effectively reducing the optical loss (absorption), inducing a shift in the emission wavelength. Allowing for completely electronic tuning, and no k-clock requirement for SS-OCT measurements.

2. SIMULATION

2.1 Working principles

Our simulation, developed in MATLAB, assumes a basic 50:50 Michelson interferometer SS-OCT setup as shown in figure 2. The sample is simplified as a complex dielectric stack with discrete refractive indices.

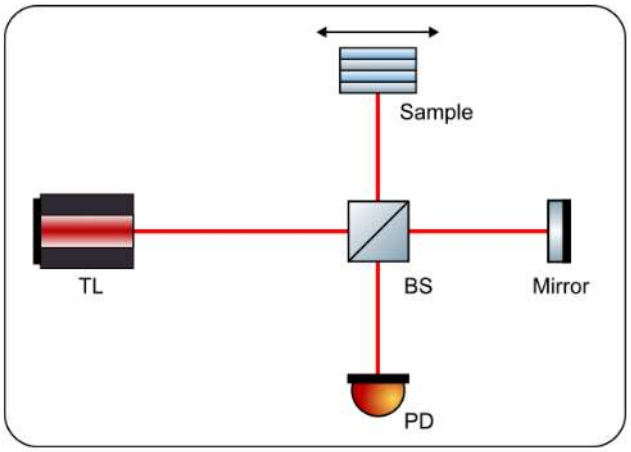

Figure 2. Schematic of basic SS-OCT setup, TL – Tunable Laser, BS – Beamsplitter, PD – Photodiode.

We model our signal in the reference arm E_r as

$$E_r(t,\omega_0) = \sqrt{A_r(\omega_0)}e^{-i(\omega_0 t)} \tag{4}$$

and our sample signal E_s as

$$E_s(t,\omega_0) = \sum_i^n \sqrt{A_s(\omega_0)}\beta_i e^{-i(\omega_0 t+\Delta\phi+\phi_i)}. \tag{5}$$

Where A_r and A_s are the amplitudes of the signals at frequency ω_0 defined by the tuning spectrum of the source, ϕ_i is the phase accumulated due to each n reflection in the sample along the optical axis, β_i represents any attenuation in the sample and $\Delta\phi$ is the difference in phase between the sample and reference signal due to reflections at the beam splitter and the ends of each arm. To model the effects of linewidth on our scan we expand our model to include mixing of frequencies around each central frequency ω_0 and modulation in the amplitude of the component frequencies due to the linewidth, such that Equations 4 and 5 become

$$E_r(t,\omega_0) = \sum_\delta^\infty \sqrt{A_r(\omega_0)\cdot A_\delta(\omega_\delta)}e^{-i(\omega_\delta t)} \tag{6}$$

and

$$E_s(t,\omega_0) = \sum_\delta^\infty\sum_i^n \sqrt{A_s(\omega_0)\cdot A_\delta(\omega_\delta)}\beta_i e^{-i(\omega_\delta t+\Delta\phi+\phi_i)}. \tag{7}$$

Where ω_δ are the frequency contributions due to the instantaneous linewidth at ω_0. A_δ is a normalised amplitude coefficient that corresponds to shape of the linewidth.

To calculate the attenuation coefficient, β_i we make the assumption that the signal field carries signal with only one reflection and the attenuation due to absorption can be calculated using Beer's Law giving

$$\beta_n = r_n\prod_i^n t_i^2\prod_i^n\sqrt{e^{-2\alpha_i L_i}}. \tag{8}$$

Where r_n is the complex reflection coefficient at the imaged interface n, t_i is the complex transmission coefficient at each interface before the imaged interface and $\sqrt{e^{-2\alpha_i L_i}}$ is the attenuation in the complex field due to the absorption α_i of each sample layer of depth L_i . Similarly, the phase accumulated by each reflection is given as

$$\phi_n = \sum_i^n 2\mu_i L_i, \tag{9}$$

where μ_i is the refractive index of each layer i. The A-scan signal on the detector is then modelled as

$$I_{out}(\omega_0) = \frac{1}{t_s}\int_{t_1}^{t_2}|E_r(t,\omega_0)+E_s(t,\omega_0)|^2 dt, \tag{10}$$

where t_s is the integrating time of the detector and $t_2 - t_1 = t_s$.

The simulation repeats the A-scan along the lateral axis of the sample and Fourier transforms the result to produce a B-scan image of the sample, the axes of which are scaled by Eq. 1 and the separation of each A-scan. It should be noted that in this simulation the scattering of light is ignored resulting in sharper images without speckle as is typically seen experimentally.

2.2 Validation of simulation

To verify the simulation we generate a 2 mm x 2 mm sample of 50 alternating layers where $\mu \in \{1.5197, 1.4978\}$, shown in figure 3a. We then specified a tuning spectrum such that $\lambda_0 = 1300$ nm, $\Delta\lambda = 120$ nm and $\delta\lambda = 0.3$ nm, and uses Eq. 1 and Eq. 2 to calibrate the depth axis of our A-scan as shown in figure 3b.

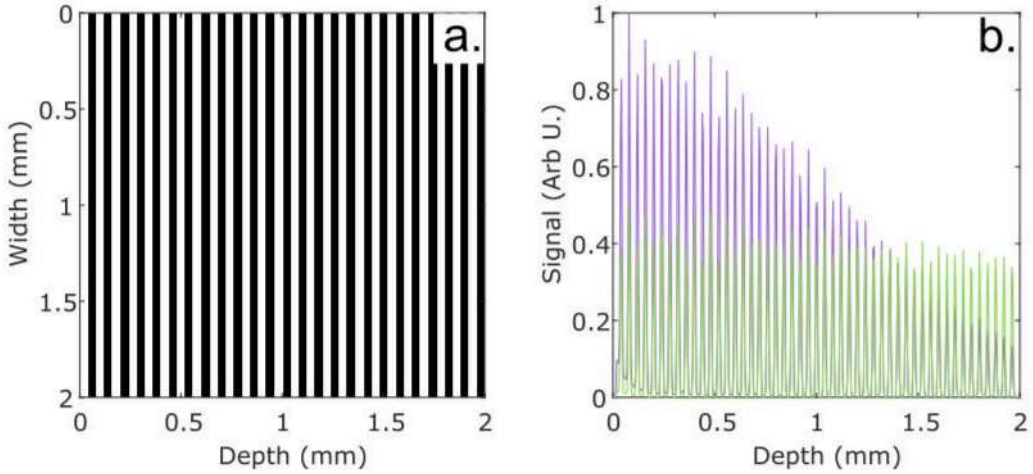

Figure 3. Output of validation run of simulation. (a) Generated sample to be interrogated, color scale shows two different refractive indices 1.5197 and 1.4978. (b) Simulated detection generated by simulation, shows detection with 0.3 nm linewidth source (purple) and 0 nm linewidth source at 50% intensity (green).

The output A-scan in figure 3b shows peaks at layer interfaces as expected. Comparing a $\delta\lambda = 0$ nm A-scan generated in parallel at 50% output we observe the 6dB point to be at 1.28 mm, a difference of 0.04mm from the result given by Eq. 3 which corresponds to the depth of the layers. From these results we verify that our simulation corresponds to the theory.

3. RESULTS

3.1 State of the art simulated performance

To contextualize the performance of our system we used the spectral properties of the 1300nm Thorlabs MEMS -VCSEL SL132121 laser in our simulation to generate a dataset for comparison. After generating the spectra according to the results in[14] and the product page for Thorlabs SL132121 we then specified a 2D resolution target of 2mm x 2mm with feature widths of 0.5mm, 0.25mm, 62.5µm, 31.3µm and 15.6µm to act as the sample in the simulation as shown in Figure 4a. Each feature was defined as a region of different refractive index where $\mu \in \{1.5197, 1.4978\}$ so that the OCT scan could resolve the interfaces between. The proximal face of the target was then padded by 0.2mm of an index matched region to allow effective delineation of Fourier artefacts from the time/depth domain scan.

Figure 4b shows, as expected, the sharp linewidth of the source results in almost zero signal attenuation at depth and the large tuning range enables the 31.3 μm features in the B-scan to be resolved. Although the SL132121 is expensive it is capable of very high detail OCT measurements which are very favorable not just for clinics but research too.

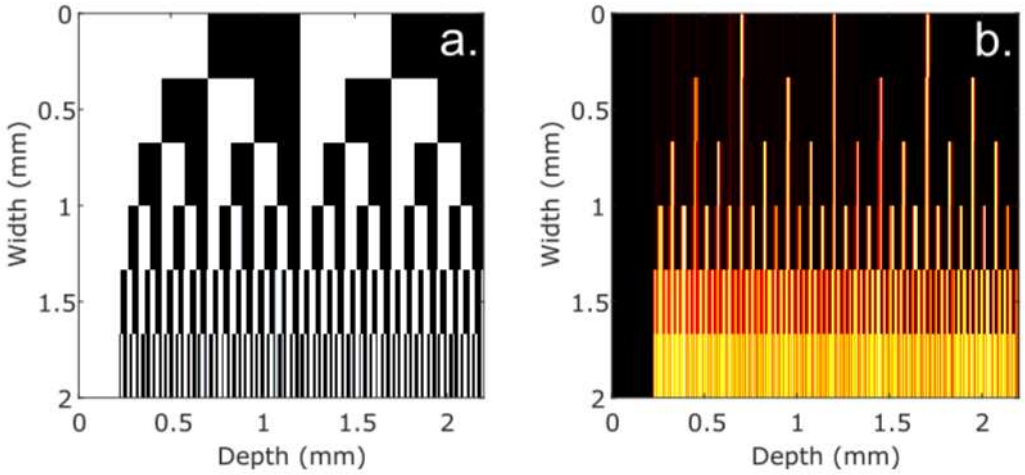

Figure 4. Output of simulation with test target and Thorlabs MEMS – VCSEL SL132121. (a) Generated resolution target, with feature widths of 0.5 mm, 0.25 mm, 62.5 μm, 31.3 μm and 15.6 μm. The color scale shows two different refractive indices 1.5197 and 1.4978. (b) Simulated detection of target with Thorlabs source.

3.2 MLLDs for OCT

First, we recorded the instantaneous output spectra of our MLLD and swept it across the tuning range recorded when selectively biasing different regions of the MLLD. This swept instantaneous spectra was then used as the input for our simulation and is shown in below in figure 5.

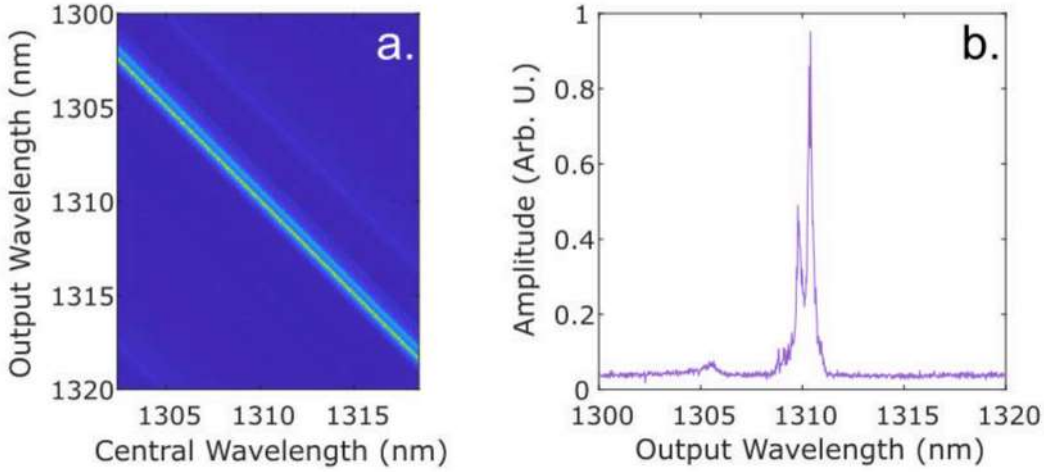

Figure 5. Experimentally obtained optical spectra from MLLD used for simulation. (a) Spectra for each central wavelength. (b) Instantaneous spectra centered at approximately 1310 nm.

Using the same target as specified before our simulations show that the B-scan in figure 6b lacks the resolution to properly resolve features beyond 62.5 μm and our current laser linewidth is limiting the signal strength beyond 1.3 mm within the sample. This is in line with our theoretical scan resolution of 35 μm.

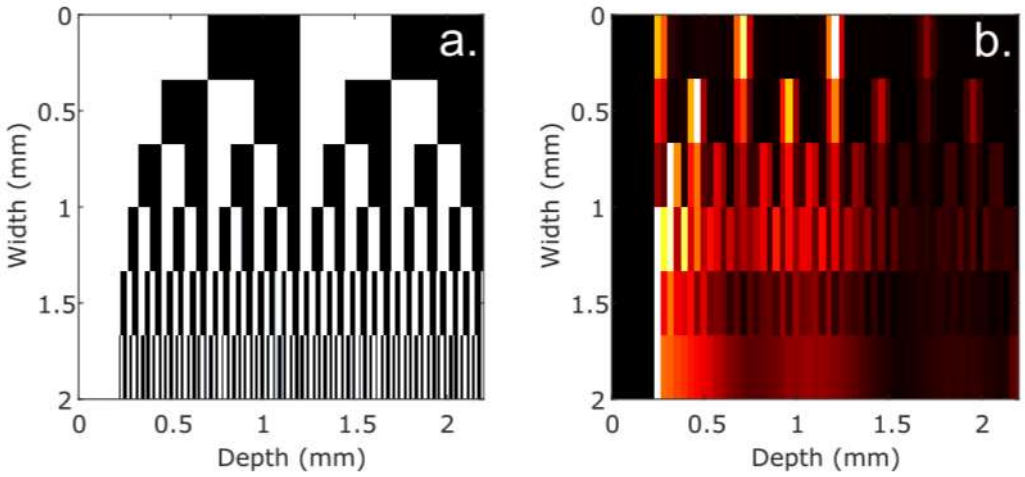

Figure 6. Output of simulation with test target and our MLLD. (a) Generated resolution target, with feature widths of 0.5mm, 0.25mm, 62.5μm, 31.3μm and 15.6μm. The color scale shows two different refractive indices 1.5197 and 1.4978. (b) Simulated detection of target with Thorlabs source.

4. DISCUSSION AND CONCLUSIONS

This difference in performance was not unexpected with the current MLLDs. These results are preliminary, and the limited tuning presents a challenge for high resolution imaging. As far as we are aware this is the first time the use of MLLDs for OCT has been investigated and we have demonstrated that the MLLDs we have grown so far would be capable of OCT. Currently we are operating in an electronically-pulsed mode which inherently requires a broad linewidth. CW operation is possible with the correct biasing, and we expect this to sharpen the output linewidth. Additionally, we have seen that we can achieve tuning that is around three times what we have shown here which in theory corresponds to a three-fold increase in resolution as well.

We consider the utilization of novel and versatile photonics devices such as MLLDs as an important step towards realizing low-cost OCT geared towards frontline clinicians that could open more efficient treatment pathways to patients. Sub-mm subsurface imaging of soft tissue with a fast, compact and all electronic system has the potential to be extremely useful to patients and clinicians alike. SD-OCT has already seen similar advances[15], and therefore a compact or handheld SS-OCT system is a feasible research goal. With an increasing research interest in artificial intelligence and machine-learning approaches to data analysis, detailed 3D images of patient problem areas could be indispensable in efficient diagnoses.

We have used the spectra from an MLLD that initially was not specified for SS-OCT and have demonstrated that it still capable of short-range scans and able to resolve features less than a 100 microns, and present the potential for MLLDs as a lesser-known key to realizing low-cost OCT systems; a concept known as a promising avenue to do this[10, 16, 17].

REFERENCES

[1] J. Welzel, E. Lankenau, R. Birngruber, and R. Engelhardt, "Optical coherence tomography of the human skin," Journal of the American Academy of Dermatology, 37(6), 958-963 (1997).

[2] M. A. Kirby, P. Tang, H.-C. Liou *et al.*, "Probing elastic anisotropy of human skin in vivo with light using non-contact acoustic micro-tapping OCE and polarization sensitive OCT," Scientific Reports, 12(1), 3963 (2022).

[3] M. Wojtkowski, V. Srinivasan, J. G. Fujimoto *et al.*, "Three-dimensional Retinal Imaging with High-Speed Ultrahigh-Resolution Optical Coherence Tomography," Ophthalmology, 112(10), 1734-1746 (2005).
[4] J. Holmes, T. von Braunmühl, C. Berking *et al.*, "Optical coherence tomography of basal cell carcinoma: influence of location, subtype, observer variability and image quality on diagnostic performance," Br J Dermatol, 178(5), 1102-1110 (2018).
[5] M. A. Choma, M. V. Sarunic, C. Yang, and J. A. Izatt, "Sensitivity advantage of swept source and Fourier domain optical coherence tomography," Optics Express, 11(18), 2183-2189 (2003).
[6] R. Chopra, S. K. Wagner, and P. A. Keane, "Optical coherence tomography in the 2020s—outside the eye clinic," Eye, 35(1), 236-243 (2021).
[7] L. S. Lim, G. Cheung, and S. Y. Lee, "Comparison of spectral domain and swept-source optical coherence tomography in pathological myopia," Eye, 28(4), 488-491 (2014).
[8] D. Bajek, and M. A. Cataluna, "Megahertz scan rates enabled by optical sampling by repetition-rate tuning," Scientific Reports, 11(1), 22995 (2021).
[9] I. Ejidike, R. A. McCracken, and D. Bajek, "Modelling two-laser asynchronous optical sampling using a single 2-section semiconductor mode-locked laser diode," Optics Express, 30(3), 3289-3301 (2022).
[10] M. Bonesi, M. P. Minneman, J. Ensher *et al.*, "Akinetic all-semiconductor programmable swept-source at 1550 nm and 1310 nm with centimeters coherence length," Optics Express, 22(3), 2632-2655 (2014).
[11] H. Wang, L. Kong, A. Forrest *et al.*, "Ultrashort pulse generation by semiconductor mode-locked lasers at 760 nm," Optics Express, 22(21), 25940-25946 (2014).
[12] D. Bajek, [High-speed optical sampling techniques enabled by ultrafast semiconductor lasers] University of Dundee, Dundee(2016).
[13] J. A. Izatt, and M. A. Choma, [Theory of Optical Coherence Tomography] Springer Berlin Heidelberg, Berlin, Heidelberg(2008).
[14] D. D. John, C. B. Burgner, B. Potsaid *et al.*, "Wideband Electrically Pumped 1050-nm MEMS-Tunable VCSEL for Ophthalmic Imaging," Journal of Lightwave Technology, 33(16), 3461-3468 (2015).
[15] G. Song, K. K. Chu, S. Kim *et al.*, "First Clinical Application of Low-Cost OCT," Translational Vision Science & Technology, 8(3), 61-61 (2019).
[16] M. Salas, M. Augustin, F. Felberer *et al.*, "Compact akinetic swept source optical coherence tomography angiography at 1060 nm supporting a wide field of view and adaptive optics imaging modes of the posterior eye," Biomedical Optics Express, 9(4), 1871-1892 (2018).
[17] J. Xu, S. Song, W. Wei, and R. K. Wang, "Wide field and highly sensitive angiography based on optical coherence tomography with akinetic swept source," Biomedical Optics Express, 8(1), 420-435 (2017).